frontiers | Frontiers in Environmental Science

ORIGINAL RESEARCH
published: 13 July 2022
doi: 10.3389/fenvs.2022.950096

Morphological Distribution and Formation Mechanisms of Antimony in the Shallow Groundwater of the Xikuangshan Antimony Mine in Hunan, China

*Ximeng Sun[1], Yi Li[2], Chao Liu[3], Lu Zhang[2], Ziyao Li[2] and Chunming Hao[1]**

[1]North China Institute of Science and Technology, Hebei, China, [2]Hebei Geo-Environment Monitoring, Hebei, China, [3]Liaoning Metallurgical Geological Exploration Research Institute Co., Ltd., Anshan, China

The century-old mining development and utilization of antimony (Sb) ore in Xikuangshan (XKS) mine, groundwater antimony pollution has attracted great attention. At present, the sources and geochemical behaviors of high Sb groundwater in this area have been widely recognized, but morphological distribution and formation mechanisms of Sb(V) and Sb(III) in shallow groundwater were still little known. Forty-three groundwater samples of Magunao aquifer (D_3x^4) were collected between June and September 2020 to determine morphological distribution and formation mechanisms of Sb valence state in the recharge area, runoff area and discharge area. The range of Sb content in the recharge area, runoff area, and discharge area of the D_3x^4 water was 3.300×10^{-3}–7.982 mg/L, 1.760×10^{-2}–17.326 mg/L and 1.230×10^{-2}–16.773 mg/L, respectively. The D_3x^4 water is dominated by Sb(V), which form was $Sb(OH)_6^-$. The Sb(V) mainly comes from the oxidative dissolution of Sb_2S_3, the mining activities, and the leaching of arsenic alkali residues. The silicate mineral weathering, carbonate mineral dissolution, and ion exchange promote the dissolution of Sb_2S_3. At the same time, redox and competitive adsorption in the runoff area increase the Sb(V) content in the water environment. The results of this research provide an understanding of the mechanism of Sb pollution in shallow groundwater and will help in controlling water-environment pollution and securing water-resource in mining areas.

Keywords: morphological characteristics, formation mechanism, valence state, antimony, shallow groundwater

OPEN ACCESS

Edited by:
Chengcheng Li,
China University of Geosciences Wuhan, China

Reviewed by:
Zhuanxi Luo,
Huaqiao University, China
Ruihua Dai,
Fudan University, China
Weihua Peng,
Suzhou University, China

****Correspondence:***
Chunming Hao
haocm@ncist.edu.cn

Specialty section:
This article was submitted to Water and Wastewater Management, a section of the journal Frontiers in Environmental Science

Received: *23 May 2022*
Accepted: *13 June 2022*
Published: *13 July 2022*

Citation:
Sun X, Li Y, Liu C, Zhang L, Li Z and Hao C (2022) Morphological Distribution and Formation Mechanisms of Antimony in the Shallow Groundwater of the Xikuangshan Antimony Mine in Hunan, China. Front. Environ. Sci. 10:950096. doi: 10.3389/fenvs.2022.950096

1 INTRODUCTION

Antimony (Sb) is a metalloid that is widespread in soil, water, and the atmosphere. It is used for producing flame retardants, semiconductor materials, and alloys (Filella et al., 2002; Anderson, 2012; Chu et al., 2019). Sb is highly toxic and carcinogenic to humans; hence, it has been listed as priority pollutant by the European Union (EU) and the United States Environmental Protection Agency (USEPA) (Hammel et al., 2000; Fu et al., 2016).

Oxidative dissolution of Sb-containing sulfides is the predominant mechanism of Sb introduction into the water environment (Casiot et al., 2007; He et al., 2012; Fu et al., 2016). Stibnite (Sb_2S_3) is the predominant Sb-containing sulfides in mining area, which are usually found in quartz veins. The

sulfur in Sb_2S_3 is oxidized when it meets oxygen in the air and water during the mining process. Sb eventually exists mainly as $Sb(OH)_6^-$, with concomitant formation of acid (Biver and Shotyk, 2012):

$$Sb_2S_3 + 7O_2 + 10H_2O = 2Sb(OH)_6^- + 8H^+ + 3SO_4^{2-} \quad (1)$$

Generally, the Sb concentration in unpolluted water is less than 1 μg/L (Filella et al., 2003; He and Wan, 2004). High levels of Sb are released into the aquatic environment by mining and smelting (Hiller et al., 2012; Wang et al., 2012; Zhou et al., 2017; He et al., 2019). The Sb concentration in a river near an Sb mine in AK, United States, was as high as 720 μg/L, while in rivers flowing 200 m downstream of a mining area in Sardinia, Italy, it reached 28 μg/L; furthermore, the Sb content of surface-water samples around a mining site in Western Carpathian Mountains (Slovakia) ranged from 1 to 9,300 μg/L (Hiller et al., 2012; Ritchie et al., 2013; Cidu et al., 2014). In China, the Sb content in an Sb mining area in Guizhou Province was as high as 1,377 μg/L (Ning et al., 2011).

In the natural environment, inorganic speciations of Sb is generally either Sb(III) or Sb(V); notably, Sb(III) is ten times more toxic than Sb(V) (Smichowski, 2008; Salam and Mohamed, 2013). Sb(V) and Sb(III) are the predominant forms of Sb in oxidized and reduced water environments, respectively. $Sb(OH)_3$, $Sb(OH)_2^+$, and SbO^+ are mainly present in acidic environments, whereas $Sb(OH)_4^-$ or aqueous SbO_2^- are present under alkaline conditions (Filella et al., 2003; Ritchie et al., 2013; Fawcett et al., 2015). Sb(III) can be adsorbed on iron-manganese oxide/hydroxide, and can be oxidized to Sb(V) in a short time. A key for the formation mechanisms of Sb(III) and Sb(V) is the instability of Sb(III) in water samples which have been in contact with atmospheric oxygen and other oxidants (Daus and Wennrich, 2014). The pH/oxidation-reduction potential (ORP) and iron-manganese oxide/hydroxide content influence the valence distribution and formation of Sb in water (Belzile et al., 2001; Leuz et al., 2006b; Wilson et al., 2010; Biver and Shotyk, 2012). The migration and transformation of Sb can also be affected by the valence (Guo et al., 2018).

Globally, Sb resources are mainly distributed in China, Russia, Bolivia, Tajikistan, South Africa, and the Mediterranean Sea (Filella et al., 2002; He et al., 2012). Primary Sb consumers are the United States, China, Japan, and the European Union (He and Wan, 2004; Qing, 2012; Tong et al., 2017). According to the statistical data from the United States Geological Survey (USGS, 2020), China's Sb production amounted to 480,000 tons, accounting for 32% of the global Sb production. Because of its vast Sb reserves, the Xikuangshan (XKS) Sb mine in the Hunan Province was named "the World's Antimony Capital" (Wang et al., 2011; Guo et al., 2018; He et al., 2019). Under the influence of mining, smelting, and other activities, the highest Sb concentration in the groundwater environment of the XKS in the Hunan Province was reported to be 29,423 μg/L, which is 5,880 times higher than the permissible Sb concentration in drinking water (i.e., 0.005 mg/L; GB5749-2022) (Zhu et al., 2009). Long-term mining activities and the accumulation of minerals and waste residues have increased the Sb contents of groundwater (Ashley et al., 2003; He, 2007; Wen et al., 2018). The sources, toxicological property, migration, and transformation of Sb, as well as the environmental risks associated with increased Sb concentration in groundwater, have been studied extensively (Guo et al., 2018; Wen et al., 2018; He et al., 2019; Zhang et al., 2022); however, there is no available systematic study on the formation mechanisms of different valence states of Sb in the oxidizing environment of shallow groundwater. Hence, further investigations regarding the impact of the environmental redox properties on the valence states of Sb are needed.

In this study, our main objectives were to analyze 1) the distribution characteristics of the Sb valence state in the recharge, runoff, and discharge areas of shallow groundwater and 2) the formation process and factors influencing the Sb valence distribution. Our results should elucidate the origin mechanisms of Sb pollutants in shallow groundwater, facilitating effective local water-environment pollution control and water-resource protection strategies in mining areas.

2 STUDY AREA

The XKS Sb mine is located between 27°49′28″–27°43′05″N and 111°25′47″–111°31′22″E near Lengshuijiang (Hunan Province, China) (**Figure 1**). The hydrogeological cross section for the study area is shown in **Figure 2**. The mine is divided into two mining areas, i.e., the north and south mines, with a total area of 26 km^2. The north mine covers an area of 0.50 km^2. The Sb reserves of the XKS Sb mine amount to more than two million tons, and there are still 400,000 tons after approximately 110 years of mining (Zhang et al., 2022).

The study area is dominated by mountain-chain strikes along the NE–SW direction. The area has a subtropical continental monsoon climate, with average annual precipitation and evaporation of 1,381 and 903 mm, respectively, while the average annual temperature is 16.70°C (reference period: 1949–2012). The Xuanshan stream and Feishuiyan and Qingfeng Rivers comprise the primary river system, which is a part of the Zijing River system.

The XKS Sb mine is located in the southern China Sb ore belt, which is in the eastern continental margin of the Yangtze Para platform and central Hunan area of the Caledonian fold belt with an axial direction of NE30–35°. F_{75} is the main fault structure, and the exposed formations are the Upper Devonian Shetianqiao (D_3s) and XKS (D_3x). The Karst fracture of the XKS Magunao (MA) aquifer (D_3x^4) has a thickness of 258 m, while the Shetianqiao (SA) aquifer (D_3s^2) has a thickness of approximately 220 m. Generally, there is no vertical hydraulic connection between these two aquifers. The Sb orebodies are mainly in the limestone section of the Shetianqiao aquifer (D_3s^2).

Being shallow groundwater, the D_3x^4 aquifer is often used as the main source of drinking water for local communities in this area.

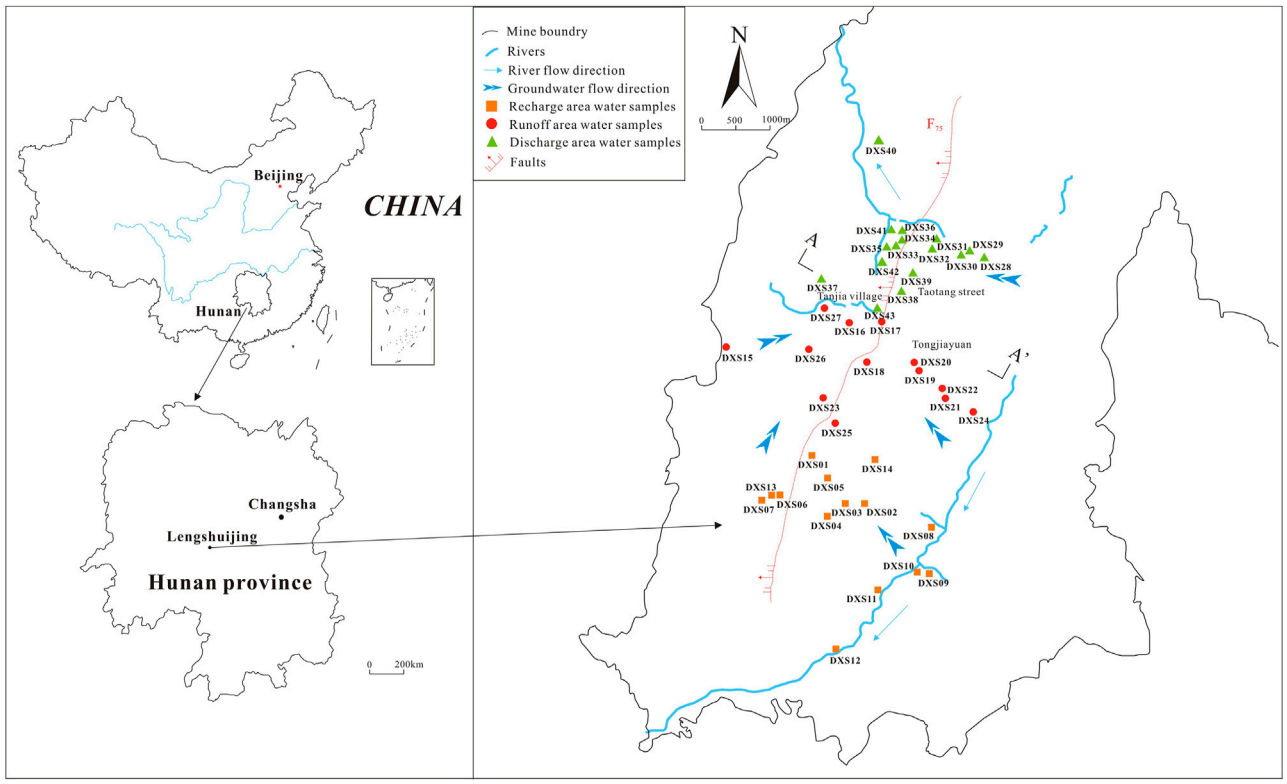

FIGURE 1 | Study area in the Hunan Province and sampling locations.

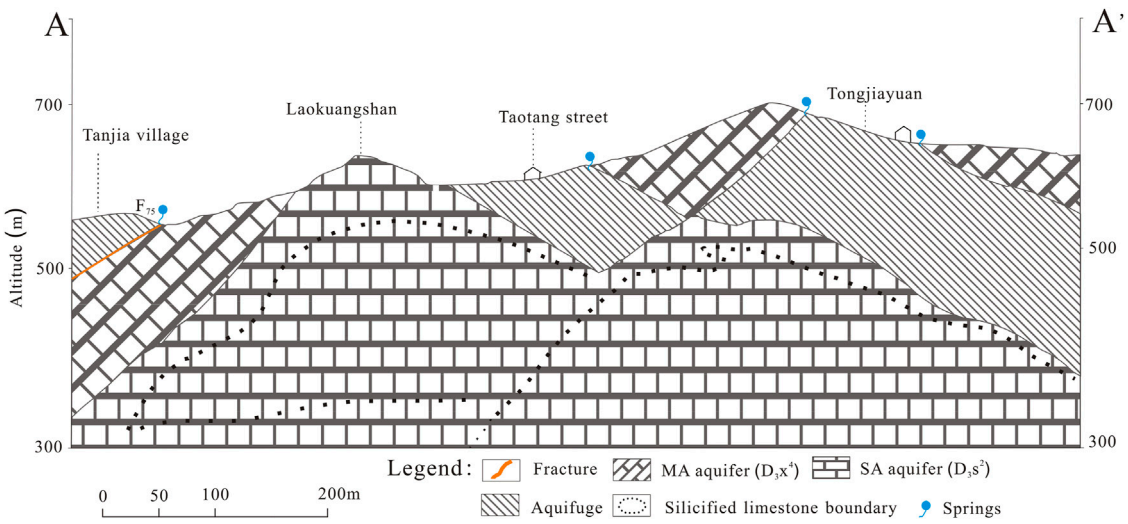

FIGURE 2 | The hydrogeological section along the A-A' line.

Moreover, the lithology of this aquifer is mainly limestone with an average permeability coefficient of 0.0092 m/d. Many springs are exposed with flow rates of 0.10–0.70 L/s. The main water source of D_3x^4 is recharge through precipitation infiltration. Groundwater flows from south to north in the interlayer fracture zone; silicified and non-silicified limestone fissures and karst caves are found in the aquifer. Water drains out mainly through springs and flows into the Qingfeng River. Residential areas and factories, as well as some waste rocks and slags from mining and smelting, are stacked above D_3x^4 (Wen et al., 2016; Xie et al., 2016).

3 MATERIALS AND METHODS

3.1 Sample Collection

A total of 43 D_3x^4 water samples from the mine area were collected between June and September 2020, including 14 recharge-area, 13 runoff-area, and 16 discharge-area water samples (**Figure 1**). Representative water samples were obtained from flowing water. Before collection, every sampling bottle was washed two to three times with distilled water and rinsed two to three times with sample water. Water samples were filtered through 0.45 μm millipore filters and stored in high-density polyethylene (HDPE) bottles. At every sampling site, three bottles of 500 ml water were collected: One bottle was the original sample, one bottle was acidified to pH < 2 with 1:1 (v/v) nitric acid for cation and trace-element analyses, and 5% (v/v) 0.25 M ethylenediamine tetraacetic acid (EDTA) was added to a third bottle of water to limit the oxidation of Sb(III) to Sb(V) during sampling (McCleskey et al., 2004; Daus and Wennrich, 2014). All sampling bottles were filled, labelled, sealed tightly, stored in a refrigerator at 4°C, and sent to the laboratory for analysis. Most indicators were analyzed and determined by the Hunan provincial institute of geological testing and research.

3.2 Sample Analysis

The pH and ORP values were measured in the field using a portable acidity meter (HANNA H18424), and the total dissolved solids (TDS) values were measured in the field using an electrical conductivity (EC) meter (HANNA H1833). The main cations (i.e., calcium, magnesium, sodium, and potassium) were measured by inductively coupled plasma atomic emission spectroscopy (ICP-AES) with a detection limit of 0.01 mg/L, whereas the main anions (i.e., chloride and sulfate) were determined by ion chromatography (Dionex ICS-1100) with an analytical precision of 0.01 mg/L. Bicarbonate and carbonate were analyzed by titration with an analysis precision of 0.1 mg/L. (Wen et al., 2018). Sb and Sb(III) concentrations were measured using a hydride generation atomic fluorescence spectrometer (HG-AFS), with an accuracy of 0.001 mg/L. The concentration of Sb(V) is the concentration of Sb minus the concentration of Sb(III) (Wang et al., 2011).

3.3 Analytical Quality Control

The analytical precision of the ion concentrations was verified by calculating the ionic balance errors. The absolute ionic balance error of water samples was < 5%. Moreover, 20% of the water samples were reanalyzed, and the error between the two results was found to be less than 10%. Each group of experiments required a blank experiment to ensure the accuracy and precision of the analytical results. All analyses were performed in triplicates; each reported value is the average of the three test results, with a relative standard deviation < 10%.

3.4 Statistics Analysis

The Origin 2021 software was used to perform all statistical analyses, including descriptive statistical analysis, Pearson correlation analysis, and principal component analysis (PCA). Piper diagram was used to elucidate the hydrogeochemical characteristics.

4 RESULTS AND DISCUSSION

4.1 Geochemical Characteristics of D_3x^4 Water

The geochemical characteristics of D_3x^4 water are presented in **Table 1**. The pH of D_3x^4 water samples ranged from 4.97 to 9.32 (mean value: 7.15), indicating that 46.76% of D_3x^4 water samples represented a weakly acidic environment. pH values ranged between 4.97 and 7.37 in the discharge area, and were lower than those in the recharge area (i.e., between 6.62 and 7.78) and runoff area (i.e., between 6.84 and 9.32).

The ORP of D_3x^4 water samples ranged from 0.04 to 0.26 V, indicating that all D_3x^4 water samples represented an oxidized environment. These findings are consistent with those of Zhu et al. (2009). Averages of ORP were 0.14, 0.18, and 0.13 V, in the recharge, runoff, and discharge areas of D_3x^4 water, respectively, i.e., the average ORP in the discharge area was lower than those in the recharge and runoff areas.

The TDS values ranged from 135 to 1,311 mg/L, with 8.90% of D_3x^4 water samples exhibiting TDS values higher than the value of the standards for drinking water (1,000 mg/L; GB5749-2022). The TDS ranges in the recharge, runoff, and discharge areas of D_3x^4 water were 151–1,311, 190–1,229, and 135–527 mg/L, respectively (mean values: 582, 595, and 311 mg/L, respectively). The higher average TDS content in the recharge and runoff areas compared with runoff area indicated that recharge and runoff areas may be affected by human activities and ion exchange between shallow groundwater and the surrounding rock (Nyirenda et al., 2015).

SO_4^{2-} was the most abundant anion in the recharge and runoff areas, with average contents of 306.76 and 272.70 mg/L, respectively, while HCO_3^- was the second anion, with average contents of 189.0 and 226.2 mg/L, respectively. The average contents of Cl^- accounted for 0.86 and 1.31% of the total anions in the recharge and runoff areas, respectively. The order of anion contents in the runoff area was as follows: SO_4^{2-} (mean value: 272.70 mg/L) > HCO_3^- (mean value: 226.2 mg/L) > Cl^- (mean value: 6.80 mg/L). The order of anion contents in the discharge area was as follows: HCO_3^-(mean value: 137.9 mg/L) > SO_4^{2-} (mean value: 137.61 mg/L) > Cl^- (mean value: 2.46 mg/L). Ca^{2+} was the most abundant cation in the D_3x^4 water samples, followed by Na^+ and Mg^{2+}. The proportions of Ca^{2+} in the recharge, runoff, and discharge areas were 68.00%, 60.56%, and 72.57%, respectively.

Along the groundwater-flow direction (**Figure 3**), the content of Ca^{2+} in D_3x^4 water exhibited a decreasing trend, while the contents of Na^+ and Mg^{2+} varied widely. The overall trend of K^+ was similar to those of Na^+ and Mg^{2+}. The anions SO_4^{2-} and HCO_3^- exhibited little changes in the recharge and runoff areas but decreased in the discharge area. Compared with the recharge area, the average contents of SO_4^{2-}, Ca^{2+}, and Mg^{2+} in the

TABLE 1 | Geochemical data of samples collected in this study.

Types	K^+	Na^+	Ca^{2+}	Mg^{2+}	Cl^-	SO_4^{2-}	HCO_3^-	CO_3^{2-}	TDS	pH	ORP
					mg/L						V
Recharge area shallow groundwater (n = 14)											
Min	0.18	0.04	32.40	1.58	0.30	59.20	78.1	0.0	151	6.62	0.08
Max	6.20	98.00	210.00	54.60	11.80	795.00	260.0	0.0	1311	7.78	0.25
Mean	2.06	29.13	105.04	18.32	4.31	306.76	189.0	0.0	582	7.25	0.14
SD	2.12	32.77	43.71	19.84	3.98	241.54	58.5	0.0	340	0.34	0.05
Runoff area shallow groundwater (n = 13)											
Min	0.26	0.32	20.40	1.58	0.31	55.30	110.0	0.0	190	6.84	0.12
Max	7.73	395.00	258.00	27.90	34.70	587.00	600.0	133.0	1229	9.32	0.26
Mean	3.01	51.94	94.80	6.80	6.80	272.70	226.2	10.2	595	7.45	0.18
SD	2.86	112.83	64.17	6.95	10.19	200.46	119.3	36.9	367	0.63	0.05
Discharge area shallow groundwater (n = 16)											
Min	0.30	0.390	14.00	1.61	0.36	47.10	9.2	0.0	135	4.97	0.04
Max	7.69	68.90	101.00	14.80	11.60	280.00	244.0	0.0	527	7.37	0.22
Mean	2.82	12.90	57.09	5.86	2.46	137.61	137.9	0.0	311	6.81	0.13
SD	2.58	20.60	27.68	3.70	2.99	66.46	79.8	0.0	129	0.63	0.04

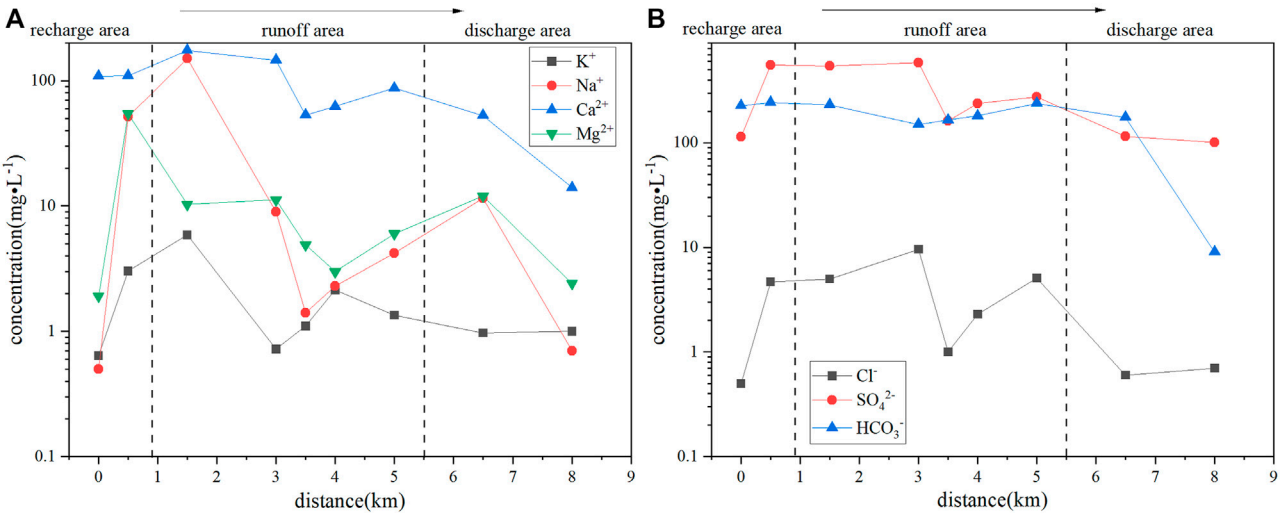

FIGURE 3 | (A) spatial distribution of Sb; **(B)** Sb cumulative percentage.

discharge area decreased by 55.14%, 45.65%, and 68.01%, respectively.

In the Piper diagram (**Figure 4**), D_3x^4 water appears dominated by Ca^{2+}, HCO_3^-, and SO_4^{2-}. The hydrochemical types in the recharge area are mainly Ca-HCO_3-SO_4 type (35.71%) and Ca-SO_4-HCO_3 type (28.57%); those in the runoff area are mainly Ca-HCO_3-SO_4 type (38.46%) and Ca-SO_4-HCO_3 type (38.46%); and the types in the discharge area are mainly Ca-HCO_3-SO_4 type (37.50%) and Ca-SO_4-HCO_3 type (25.00%).

4.2 Morphological Characteristics of Antimony in D_3x^4 Water

As shown in **Table 2**, in the recharge area of D_3x^4 water, the Sb(III) content ranged from 2.000×10^{-4} to 0.282 mg/L (mean value: 0.066 mg/L), the Sb(V) content ranged from 3.100×10^{-3} to 7.700 mg/L (mean value: 1.962 mg/L), while the Sb content ranged from 3.300×10^{-3} to 7.982 mg/L (mean value: 2.028 mg/L). In the runoff area, the Sb(III) content ranged from 1.200×10^{-3} to 0.726 mg/L (mean value: 0.116 mg/L), the Sb(V) content ranged from 1.610×10^{-2} to 16.600 mg/L (mean value: 3.328 mg/L), and the Sb content ranged from 1.760×10^{-2} to 17.326 mg/L (mean value: 3.445 mg/L). In the discharge area, the content of Sb(III) ranged from 6.000×10^{-4} to 0.573 mg/L (mean value: 0.078 mg/L), the content of Sb(V) ranged from 1.170×10^{-2} to 16.200 mg/L (mean value: 2.499 mg/L), and the content of Sb ranged from 1.230×10^{-2} to 16.773 mg/L (mean value: 2.577 mg/L). The Sb content values in the shallow groundwater of the XKS Sb mine were lower than those reported by Xie et al. (2016) and Wen et al. (2018). The average Sb contents in the recharge, runoff, and discharge

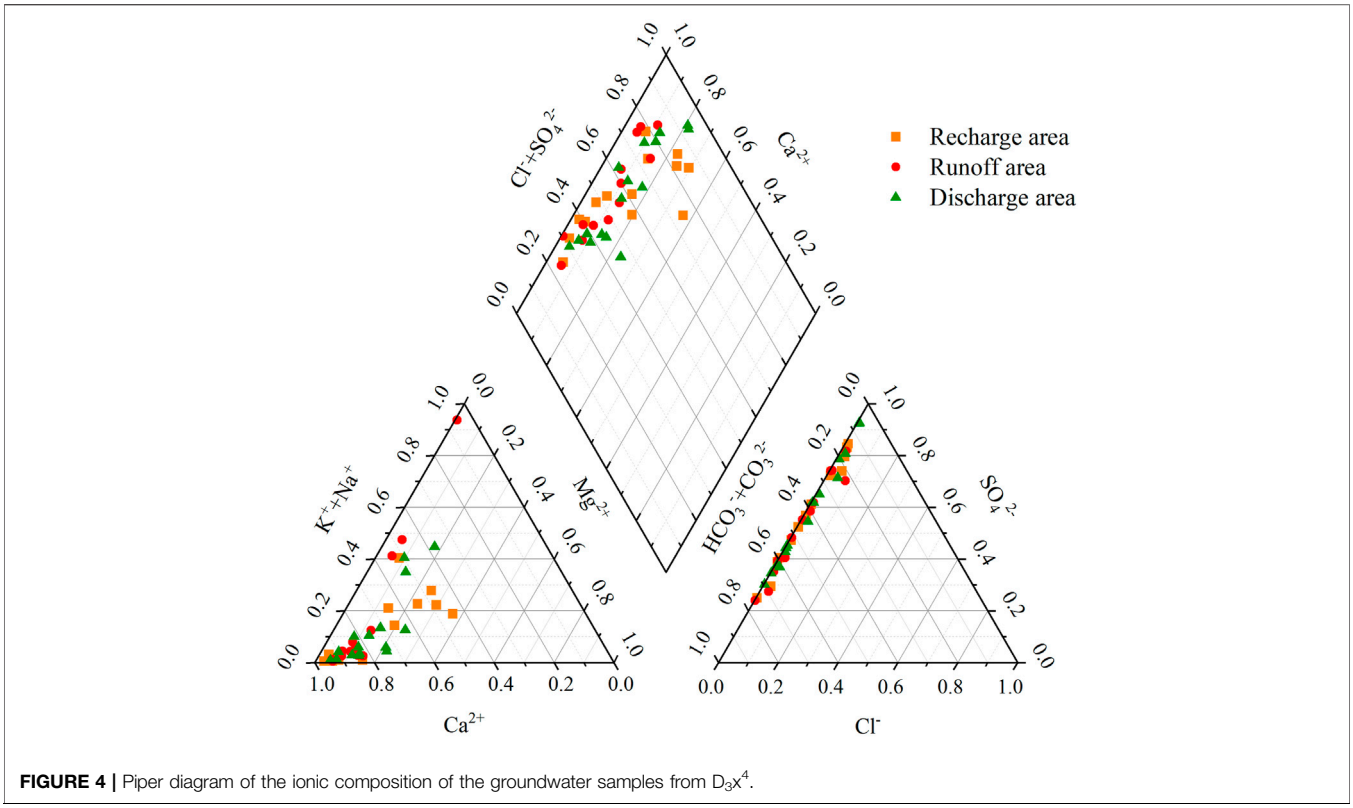

FIGURE 4 | Piper diagram of the ionic composition of the groundwater samples from D_3x^4.

TABLE 2 | Concentrations of Sb in this study.

Types	Sb(III)	Sb(V)	Sb
		mg/L	
Recharge area shallow groundwater (n = 14)			
Min	2.000×10^{-4}	3.100×10^{-3}	3.300×10^{-3}
Max	0.282	7.700	7.982
Mean	0.066	1.962	2.028
SD	0.098	2.824	2.921
Runoff area shallow groundwater (n = 13)			
Min	1.200×10^{-3}	1.610×10^{-2}	1.760×10^{-2}
Max	0.726	16.600	17.326
Mean	0.116	3.328	3.445
SD	0.220	5.603	5.818
Discharge area shallow groundwater (n = 16)			
Min	6.000×10^{-4}	1.170×10^{-2}	1.230×10^{-2}
Max	0.573	16.200	16.773
Mean	0.078	2.499	2.577
SD	0.145	4.391	4.534

areas were 405, 687, and 515 times greater, respectively, than the limit defined by China's national drinking water quality guidelines (i.e., 0.005 mg/L).

As shown in **Table 2** and **Figure 5**, the Sb(V) contents in the recharge, runoff, and discharge areas were higher than those of Sb(III), suggesting that D_3x^4 water was dominated by Sb(V). The spatial distribution of Sb (**Figure 5A**) revealed that, along with the groundwater flow, the contents of Sb(III), Sb(V), and Sb first increased, then decreased, and then increased again. The changing trends of Sb and Sb(V) were similar, indicating that the geochemical behavior of Sb was mainly controlled by Sb(V).

4.3 Formation Mechanisms

4.3.1 Relationship Between Antimony and Geochemical Factors

Figure 6A reveals the positive correlations between the Sb and SO_4^{2-} contents in the recharge and runoff areas, with R^2 = 0.76 and 0.55, respectively, indicating the dissolution of Sb-bearing sulfide minerals. Sb_2S_3 is the main ore mineral of Sb in the XKS Sb mine (Fan et al., 2004).

In the Sb_2S_3 oxidation reaction, Sb/SO_4^{2-} satisfies the 2:3 relationship (**Eq. 1**). In **Figure 6A**, all water samples are from below the Sb_2S_3 oxidation-reaction line, with the high SO_4^{2-} content indicating the dissolution of other sulfate minerals, such as pyrite (Casiot et al., 2007; Wen et al., 2016; Guo et al., 2018). However, the correlation between the Sb and SO_4^{2-} contents in the discharge area was not obvious, indicating that the dissolution of Sb-bearing sulfide minerals had little influence on the change of Sb content in the discharge area (**Figure 6A**). The distributions of Sb(V) and Sb contents were similar, indicating that the recharge, runoff, and discharge of D_3x^4 water were mainly controlled by Sb(V).

Figure 6B shows that the positive correlation between Sb and Cl^- in the runoff area, indicating that the influence of anthropogenic activities on the increase of Sb content in the runoff area can not be ignored (Hao et al., 2021). The Sb content exhibited stronger positive correlations with the contents of HCO_3^-, and TDS in the runoff area than in the recharge and

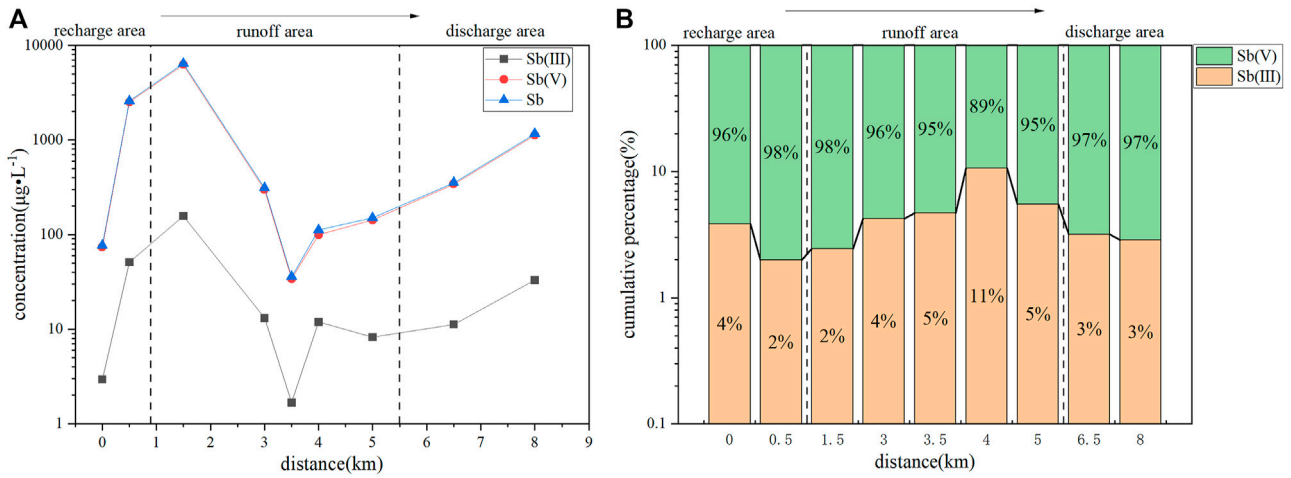

FIGURE 5 | (A) Spatial distribution of cations; **(B)** spatial distribution of anions.

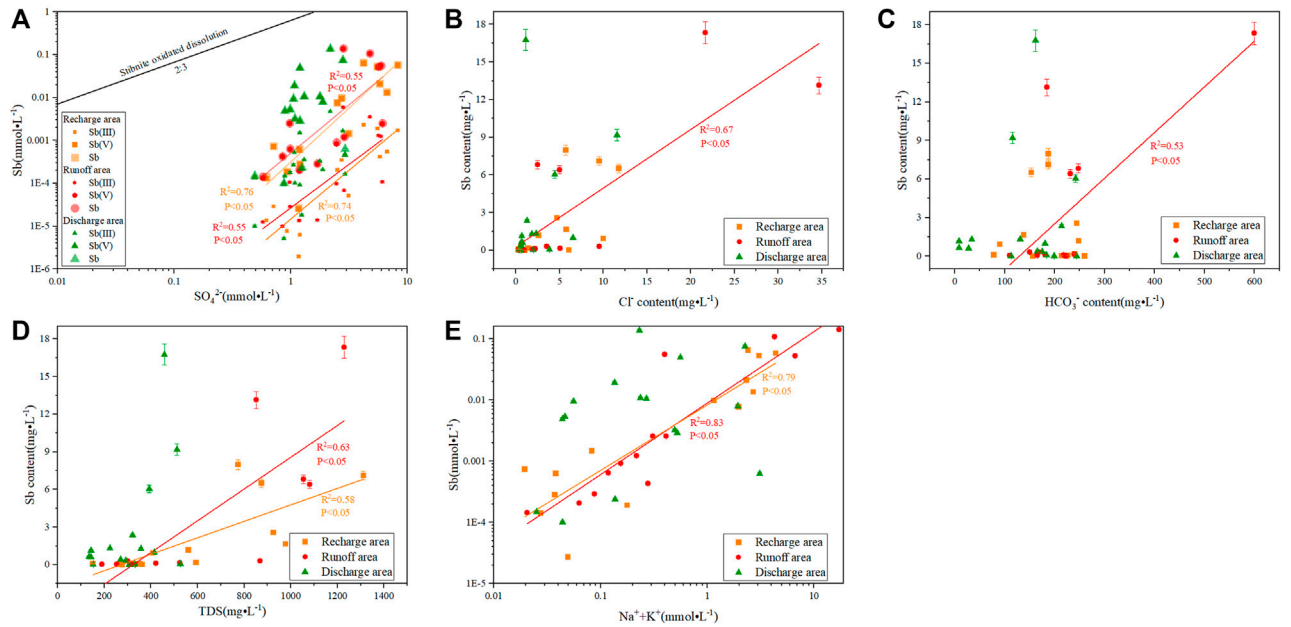

FIGURE 6 | Relationships between Sb content and the geochemical characteristics of the water samples: **(A)** Sb versus SO_4^{2-}; **(B)** Sb versus Cl^-; **(C)** Sb versus HCO_3^-; **(D)** Sb versus TDS; **(E)** Sb versus $Na^+ + K^+$.

discharge areas (**Figures 6C,D**), indicating that a strong water–rock interaction can promote the dissolution of carbonate minerals and neutralize the H^+ generated by the dissolution of Sb_2S_3. This accelerates the oxidative dissolution of Sb_2S_3 in a weakly alkaline environment (Biver and Shotyk, 2012; Nyirenda et al., 2015), and generates Sb(V) in the form of $Sb(OH)_6^-$, thereby promoting the content of Sb.

Figure 6E shows that Sb and Na^++K^+ were more strongly correlated in the recharge and runoff areas (R^2: 0.79 and 0.83, respectively) than in the discharge area of D_3x^4 water, indicating that the increase in Sb content in the recharge and runoff areas was related to the dissolution of Na-containing minerals and ion exchange. The arsenic-alkali residues produced by Sb smelting was the main Na-containing mineral in the study area, and Sb existed in the form of Na_3SbO_4, $NaSbS_2$, and Na_3SbS_4 (Deng et al., 2014; Long et al., 2020). The chemical reactions are as follows:

$$Na_3SbO_4 + 4H_2O = Sb(OH)_6^- + 2OH^- \quad (2)$$

$$NaSbS_2 + 4O_2 + 3H_2O = Sb(OH)_3 + 2SO_4^{2-} + 3H^+ \quad (3)$$

$$2Sb(OH)_3 + O_2 + 4H_2O = 2Sb(OH)_6^- + 2H^+ \quad (4)$$

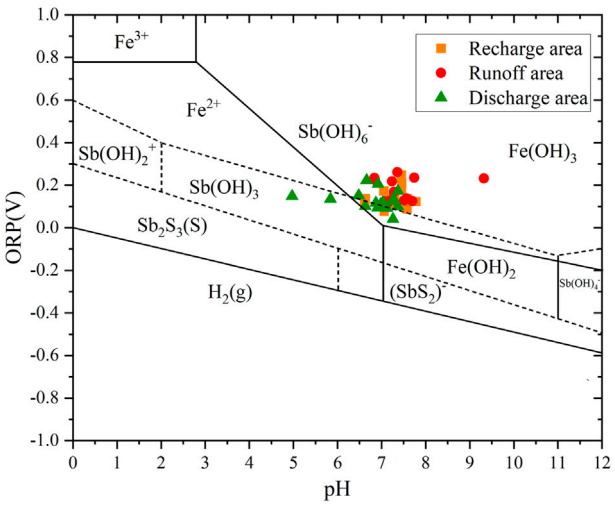

FIGURE 7 | Relationship between pH and ORP for all shallow groundwater samples.

$$Na_3SbS_4 + 8O_2 + 6H_2O = Sb(OH)_6^- + 4SO_4^{2-} + 6H^+ \quad (5)$$

4.3.2 Redox Process

In oxidizing water, when pH ranged between 4.50 and 6.50, Sb existed in the form of $Sb(OH)_3$; when pH ranged between 6.50 and 8.00, Sb(V) was the main form, existing mainly in the form of anion $Sb(OH)_6^-$, while only a small part of Sb(III) existed, in which Sb existed in the recharge and discharge areas as $Sb(OH)_3$ and $Sb(OH)_6^-$, and in the runoff area as $Sb(OH)_6^-$; when pH was greater than 8.00, Sb existed in the form of $Sb(OH)_6^-$ (**Figure 7**).

The poor correlations between Sb content and ORP in the recharge, runoff, and discharge areas (**Figure 8A**) suggested that the ORP values had little effect on the morphology of Sb. The Sb(V) content in the runoff area was moderately correlated with pH, whereas the Sb contents in the recharge and discharge areas were poorly correlated with pH (**Figure 8B**). Therefore, pH affected the presence of Sb valence in the runoff area, while its impact on the presence of Sb in the recharge and discharge areas can be ignored.

The main form of Sb in rocks or minerals was Sb(III); however, in the water bodies surrounding the Sb ore areas, Sb was mainly in the form of Sb(V) (Casiot et al., 2007; Multani et al., 2016). This indicated that Sb would migrate in the form of Sb(III) from rocks and minerals to the water body, where Sb(III) would oxidize to Sb(V) (Ashley et al., 2003). After the mining activity in the study area, O_2 would enter the underground goaf, thereby changing the groundwater environment in the recharge, runoff, and discharge areas from a reduced to an oxidized state and providing sufficient conditions for mineral oxidation. Sb(III) and Sb(V) were positively correlated with SO_4^{2-} in the recharge and runoff areas, with 0.74, 0.76, 0.55, and 0.55 correlation coefficients, respectively (**Figure 6A**), indicating that Sb_2S_3 in the ore seam would undergo an oxidation reaction upon contact with oxygen during the mining process. In the system with coexisting Sb and iron (Fe), Fe(II), and Fe(III) promoted the oxidation of Sb(III) through a catalytic reaction in an acidic water environment (Leuz et al., 2006a; Jiang et al., 2020). With a pH increase, the main form of Fe in the study area would be $Fe(OH)_3$, Fe-assisted oxidation would weaken, pH would play the main role, Sb(III) would be hydrolyzed in eutrophic water, and the content of $Sb(OH)_4^-$ would increase, while $Sb(OH)_4^-$ would oxidize to form $Sb(OH)_6^-$ (Leuz et al., 2006b; Multani et al., 2016; Liu et al., 2021). The reactions are as follows:

$$Sb_2S_3 + 6O_2 + 3H_2O = Sb_2O_3 + 3SO_4^{2-} + 6H^+ \quad (6)$$

$$Sb_2O_3 + 3H_2O = 2Sb(OH)_3 \quad (7)$$

$$Sb(OH)_3 + H_2O = H^+ + Sb(OH)_4^- \quad (8)$$

$$2Sb(OH)_4^- + O_2 + 2H_2O = 2Sb(OH)_6^- \quad (9)$$

4.3.3 Principal Component Analysis

PCA data were showed in **Table 3**, the cumulative contribution rate was obtained by extracting the initial

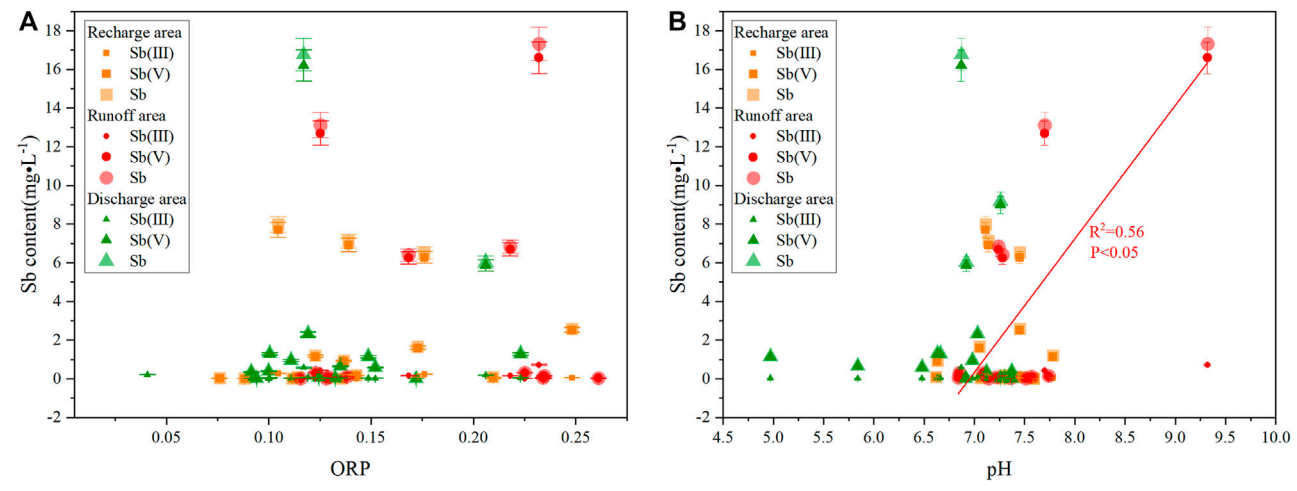

FIGURE 8 | (A) ORP versus Sb; **(B)** pH versus Sb.

TABLE 3 | Principal component analysis in the study area.

Ingredient	Elements	Initial eigenvalues			Extract sum of squares		
		Total	Variance %	Accumulation %	Total	Variance %	Accumulation %
1	Sb	4.50	44.98	44.98	4.49	44.98	44.98
2	K^+	2.39	23.88	68.86	2.39	23.88	68.86
3	Na^+	1.30	13.01	81.87	1.30	13.01	81.87
4	Ca^{2+}	0.62	6.24	88.11			
5	Mg^{2+}	0.46	4.63	92.74			
6	Cl^-	0.33	3.29	96.03			
7	SO_4^{2-}	0.20	2.06	98.09			
8	HCO_3^-	0.112	1.12	99.21			
9	CO_3^{2-}	0.05	0.52	99.73			
10	pH	0.03	0.27	100			

TABLE 4 | Composition matrix and common factor variance in the study area.

Elements	Ingredient		
	1	2	3
Sb	0.78	−0.02	−0.39
K^+	0.63	0.33	−0.49
Na^+	0.87	0.32	−0.10
Ca^{2+}	0.40	0.70	0.42
Mg^{2+}	0.41	0.74	0.21
Cl^-	0.75	−0.04	−0.41
SO_4^{2-}	0.64	0.70	0.04
HCO_3^-	0.72	−0.38	0.52
CO_3^{2-}	0.67	−0.64	0.03
pH	0.69	−0.32	0.54

eigenvalues in the element correlation-coefficient matrix for D_3x^4 water. Following the principle according to which the total of the initial eigenvalues is greater than unity, three common factors with eigenvalues greater than unity when analyzing the Sb pollution source were found 81.87% of the pollution source information in D_3x^4 water, indicating that the extraction of three common factors satisfied the principal components, which could represent key hydrochemical characteristics.

According to the PCA matrix (**Table 4**; **Figure 9**), factor 1 (49.98%) was predominantly loaded on Sb, K^+, Na^+, Cl^-, HCO_3^-, and CO_3^{2-}. The primary sources of Sb were influenced by rock weathering, anthropogenic processes, especially the mining activities, leaching of arsenic-alkali residues, and ion-exchange interactions.

Some water samples from the recharge area of D_3x^4 water were from the dominant rock-weathering field and were mainly affected by silicate weathering in **Supplementary Figure S3** (Zhu et al., 2011; Xing et al., 2013). At the same time, the water samples from the recharge area tended to go from the dominant rock-weathering field to the dominant evaporation/concentration field. Previous studies have found abundant silicified limestones in this area, whose main mineral components are quartz and low-temperature albite ($NaAl_2Si_3O_8$) (Hao et al., 2020a). The reactions of the silicate water–rock interaction are the following:

$$2NaAl_2Si_3O_8 + 2CO_2 + 11H_2O = Al_2Si_2O_5(OH)_4 + 2Na^+ + 4H_4SiO_4 + 2HCO_3^- \quad (10)$$

$$2NaAl_2Si_3O_8 + 2H^+ + 9H_2O = Al_2Si_2O_5(OH)_4 + 2Na^+ + 4H_4SiO_4 \quad (11)$$

The D_3x^4 water samples in the runoff and discharge areas were mainly located in the dominant rock-weathering field (**Supplementary Figure S4**), and the water–rock interaction was jointly controlled by the weathering of silicate minerals and dissolution of carbonate minerals (**Supplementary Figure S4**) (Gibbs, 1970; Belkhiri et al., 2010; Liu et al., 2016). The dissolution of carbonate and silicate minerals would promote the Sb_2S_3 reaction and increase the Sb(V) content. Some water samples in the recharge and runoff areas were outside the Gibbs diagram, indicating that they may also have been affected by human activities (Thomas et al., 2013). At the same time, the presence of Cl^- indicates the influence of anthropogenic activities (Hao et al., 2021).

The presence of K^+ and Na^+ indicated the leaching of arsenic-alkali residues and the effect of ion-exchange interactions (Xiao et al., 2015; Jia et al., 2020). The increase in Sb content in the recharge and runoff areas was affected by the leaching of arsenic-alkali residues (**Figure 6E**). The production of arsenic-alkali residues are mainly influenced by mining activities, so the source and content of Sb in the recharge and runoff areas were also influenced by the mining activities (Long et al., 2020). The study area is affected by long-term mining activities, as well as the effect of solid wastes, such as domestic and mining wastes (Wen et al., 2016; Guo et al., 2018; Hao et al., 2020a). Further, calcium, magnesium, and other substances in the soil are replaced through oxidative decomposition under the effects of light, oxygen, plants, and microorganisms. After their release, under the influence of rainwater erosion and surface runoff, they enter the groundwater, and Ca^{2+} and Mg^{2+} have reverse cation exchanges with K^+ and Na^+ in the surrounding rock, which increase the content of K^+ and Na^+ in the water (**Supplementary Figure S5**) (Xing et al., 2013; Liu et al., 2019; Hao et al., 2021). Along the groundwater-flow direction, from the recharge area to the runoff area, the Na^+ content first increased and then decreased; from the runoff area to the

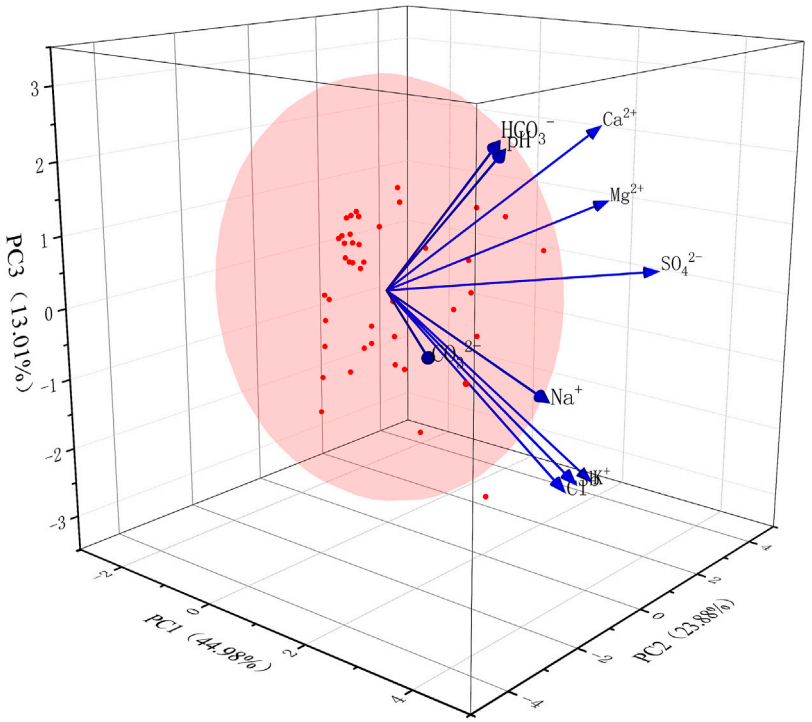

FIGURE 9 | Composition diagram for the groundwater from D_3x^4.

discharge area, the Na^+ content first increased and then decreased (**Figure 3A**). This result may be related to ion exchange (Hao et al., 2020b). Ion exchange occurred in the recharge, runoff, and discharge areas of D_3x^4 in the study area (**Supplementary Figure S6**). Owing to rock weathering, mining activities, waste-rock residues, and domestic garbage accumulation in the XKS Sb mining area in Hunan, Sb-containing pollutants would enter the shallow groundwater through rainwater erosion and surface runoff, thereby increasing the Sb(V) content in the D_3x^4 water.

Factor 2 (23.88%) was predominantly loaded on Ca^{2+}, Mg^{2+}, and SO_4^{2-}, indicating carbonate and silicate mineral dissolutions and cation exchange (Hao et al., 2021). Mineral dissolution controls the chemical composition of water in recharge and discharge areas (**Supplementary Figure S7**).

Factor 3 (13.01%) was dominated by HCO_3^- and pH, which were affected by competitive adsorption and redox. HCO_3^- can reduce the effective adsorption sites of the adsorbent through competitive adsorption, thereby affecting the attachment of Sb to minerals. Generally, a high HCO_3^- concentration leads to stronger competitive adsorption; thus, the released Sb(V) content increases (Wang et al., 2018; Hao et al., 2021). **Figure 6C** shows that the Sb content in the runoff area was positively correlated with HCO_3^- ($R^2 = 0.53$), while there was no obvious correlation between the recharge and the discharge areas. The HCO_3^- content and the corresponding Sb content in the runoff area were higher than those in the recharge and discharge areas (**Tables 1**, **2**), indicating that the HCO_3^- competitive adsorption in the runoff area promoted an increase in Sb(V) content.

The pH had no effect on the adsorption of Sb(III), and the adsorption of Sb(V) decreased with increasing pH. Generally, Sb is adsorbed on Fe oxides, and with a pH increase, Fe mainly exists in the form of $Fe(OH)_3$ precipitation in the water environment; the adsorption is weakened, desorption occurs, and Sb is released into the water environment (Flynn et al., 2003; Wilson et al., 2010; Loni et al., 2020). $Fe(OH)_3$ has no effect on Sb(III) oxidation, and high pH promotes the hydrolysis of Sb(III) to form Sb(V). In this case, the pH affected the increase in Sb(V) content in the runoff area (**Figure 8B**).

The contribution rates of PCA1, PCA2, and PCA3 were 49.98%, 23.88%, and 13.01%, respectively. The contribution rate of PCA1 was higher than those of the other two principal components, so the main source of Sb contamination in D_3x^4 water was mainly influenced by the source of PCA1, i.e., Sb_2S_3 oxidative dissolution, mining activities, and arsenic-alkali residue leaching. The formation mechanism of Sb in the recharge area was mainly affected by silicate mineral weathering, mineral dissolution, and ion exchange; in the runoff area, it was mainly affected by mineral dissolution, competitive adsorption, ion exchange, and redox; and in the discharge area, it was mainly affected by mineral dissolution and ion exchange. The effect of ion-exchange interaction on the composition of shallow groundwater in the runoff and discharge areas was higher than that of mineral dissolution.

5 CONCLUSION

The distribution characteristics and formation mechanisms of the different Sb valence states were studied by analyzing the content

of Sb(III), Sb(V), and Sb in the groundwater in the recharge, runoff, and discharge areas of D_3x^4 water. The main conclusions are as follows:

(1) The ranges of Sb content in the recharge, runoff, and discharge areas of D_3x^4 water were 3.300×10^{-3}–7.982, 1.760×10^{-2}–17.326, and 1.230×10^{-2}–16.773 mg/L, respectively (mean values: 2.028, 3.445, and 2,577 mg/L, respectively), which were 405, 687, and 515 times greater, respectively, than the permissible limit according to China's national drinking water quality guidelines (i.e., 0.005 mg/L; GB5749-2022).
(2) The average Sb(V) content was higher than that of Sb(III) in the recharge, runoff, and discharge areas of D_3x^4. D_3x^4 water was dominated by Sb(V), which was present in the form of $Sb(OH)_6^-$.
(3) The Sb(V) in the groundwater of D_3x^4 mainly originated from the oxidative dissolution of Sb_2S_3, the mining activities, and the leaching of arsenic-alkali residues. Silicate mineral weathering, carbonate mineral dissolution, and ion exchange in the recharge, runoff, and discharge areas promote the dissolution of Sb_2S_3. At the same time, affected by redox and competitive adsorption in the runoff area, Sb(III) can be hydrolyzed, and Sb(V) can be desorbed, increasing the Sb(V) content.

About the environmental implication with limitation, due to limited experimental conditions, this paper only studied the part of inorganic Sb. However, organic Sb also has a great impact on the environment, which requires further research.

DATA AVAILABILITY STATEMENT

The original contributions presented in the study are included in the article/**Supplementary Material**, further inquiries can be directed to the corresponding author.

AUTHOR CONTRIBUTIONS

Conceptualization, methodology, and writing- original draft preparation, XS; data curation, visualization, and investigation, YL and CL; software and investigation, LZ and ZL; supervision, writing- reviewing, and editing, CH. All authors contributed to manuscript revision, read, and approved the submitted version.

FUNDING

This work was supported by the Natural Science Foundation of Hebei Province (D2021508004), the Open Fund of State Key Laboratory of Groundwater Protection and Utilization by Coal Mining (Grant number SHJT-17-42.17), and the ecological restoration project in the Lengshuijiang antimony mine area (Grant LCG2020009).

SUPPLEMENTARY MATERIAL

The Supplementary Material for this article can be found online at: https://www.frontiersin.org/articles/10.3389/fenvs.2022.950096/full#supplementary-material

REFERENCES

Anderson, C. G. (2012). The Metallurgy of Antimony. *Geochemistry* 72, 3–8. doi:10.1016/j.chemer.2012.04.001

Ashley, P. M., Craw, D., Graham, B. P., and Chappell, D. A. (2003). Environmental Mobility of Antimony Around Mesothermal Stibnite Deposits, New South Wales, Australia and Southern New Zealand. *J. Geochem. Explor.* 77 (1), 1–14. doi:10.1016/s0375-6742(02)00251-0

Belkhiri, L., Boudoukha, A., Mouni, L., and Baouz, T. (2010). Application of Multivariate Statistical Methods and Inverse Geochemical Modeling for Characterization of Groundwater - A Case Study: Ain Azel Plain (Algeria). *Geoderma* 159 (3-4), 390–398. doi:10.1016/j.geoderma.2010.08.016

Belzile, N., Chen, Y.-W., and Wang, Z. (2001). Oxidation of Antimony (III) by Amorphous Iron and Manganese Oxyhydroxides. *Chem. Geol.* 174 (4), 379–387. doi:10.1016/s0009-2541(00)00287-4

Biver, M., and Shotyk, W. (2012). Stibnite (Sb2S3) Oxidative Dissolution Kinetics from pH 1 to 11. *Geochimica Cosmochimica Acta* 79, 127–139. doi:10.1016/j.gca.2011.11.033

Casiot, C., Ujevic, M., Munoz, M., Seidel, J. L., and Elbaz-Poulichet, F. (2007). Antimony and Arsenic Mobility in a Creek Draining an Antimony Mine Abandoned 85 Years Ago (Upper Orb Basin, France). *Appl. Geochem.* 22 (4), 788–798. doi:10.1016/j.apgeochem.2006.11.007

Chu, J., Mao, J., and He, M. (2019). Anthropogenic Antimony Flow Analysis and Evaluation in China. *Sci. Total Environ.* 683, 659–667. doi:10.1016/j.scitotenv.2019.05.293

Cidu, R., Biddau, R., Dore, E., Vacca, A., and Marini, L. (2014). Antimony in the Soil-Water-Plant System at the Su Suergiu Abandoned Mine (Sardinia, Italy): Strategies to Mitigate Contamination. *Sci. Total Environ.* 497-498, 319–331. doi:10.1016/j.scitotenv.2014.07.117

Daus, B., and Wennrich, R. (2014). Investigation on Stability and Preservation of Antimonite in Iron Rich Water Samples. *Anal. Chim. Acta* 847, 44–48. doi:10.1016/j.aca.2014.08.019

Deng, W., Chai, L., and Dai, Y. (2014). Industrial Experimental Study on Comprehensive Recoverying Valuable Resources from Antimony Smelting Arsenic Alkali Residue. *Hunan Nonferrous Met.* 30 (3), 24–27. doi:10.3969/j.issn.1003-5540.2014.03.007

Fan, D., Zhang, T., and Ye, J. (2004). The Xikuangshan Sb Deposit Hosted by the Upper Devonian Black Shale Series, Hunan, China. *Ore Geol. Rev.* 24 (1-2), 121–133. doi:10.1016/j.oregeorev.2003.08.005

Fawcett, S. E., Jamieson, H. E., Nordstrom, D. K., and McCleskey, R. B. (2015). Arsenic and Antimony Geochemistry of Mine Wastes, Associated Waters and Sediments at the Giant Mine, Yellowknife, Northwest Territories, Canada. *Appl. Geochem.* 62, 3–17. doi:10.1016/j.apgeochem.2014.12.012

Filella, M., Belzile, N., and Chen, Y.-w. (2002). Antimony in the Environment: a Review Focused on Natural Waters I. Occurrence. *Earth-Sci. Rev.* 57 (1-2), 125–176. doi:10.1016/s0012-8252(02)00089-2

Filella, M., Belzile, N., and Chen, Y.-W. (2003). Antimony in the Environment: A Review Focused on Natural Waters. Part 2. Relevant Solution Chemistry. *ChemInform* 34 (1-4), 265–285. doi:10.1002/chin.200323280

Flynn, H. C., Meharg, A. A., Bowyer, P. K., and Paton, G. I. (2003). Antimony Bioavailability in Mine Soils. *Environ. Pollut.* 124 (1), 93–100. doi:10.1016/s0269-7491(02)00411-6

Fu, Z., Wu, F., Mo, C., Deng, Q., Meng, W., and Giesy, J. P. (2016). Comparison of Arsenic and Antimony Biogeochemical Behavior in Water, Soil and Tailings from Xikuangshan, China. *Sci. Total Environ.* 539, 97–104. doi:10.1016/j.scitotenv.2015.08.146

Gibbs, R. J. (1970). Mechanisms Controlling World Water Chemistry. *Science* 170 (3962), 1088–1090. doi:10.2307/1730827

Guo, W., Fu, Z., Wang, H., Song, F., Wu, F., and Giesy, J. P. (2018). Environmental Geochemical and Spatial/temporal Behavior of Total and Speciation of

Antimony in Typical Contaminated Aquatic Environment from Xikuangshan, China. *Microchem. J.* 137, 181–189. doi:10.1016/j.microc.2017.10.010

Hammel, W., Debus, R., and Steubing, L. (2000). Mobility of Antimony in Soil and its Availability to Plants. *Chemosphere* 41 (11), 1791–1798. doi:10.1016/S0045-6535(00)00037-0

Hao, C., Gui, H., Sheng, L., Miao, J., and Lian, H. (2021). Contrasting Water-Rock Interaction Behaviors of Antimony and Arsenic in Contaminated Rivers Around an Antimony Mine, Hunan Province, China. *Geochemistry* 81 (2), 125748. doi:10.1016/j.chemer.2021.125748

Hao, C., Zhang, W., and Gui, H. (2020a). Hydrogeochemistry Characteristic Contrasts between Low- and High-Antimony in Shallow Drinkable Groundwater at the Largest Antimony Mine in Hunan Province, China. *Appl. Geochem.* 117, 104584. doi:10.1016/j.apgeochem.2020.104584

Hao, Q., Xu, X., Zhang, X., and Zhou, L. (2020b). Hydrochemical Characteristics and Genesis of High-Fluorine Shallow Groundwater in Yanggu Area of the Northwestern Shandong, Chin. *J. Earth Sci. Environ.* 42 (5), 668–677. doi:10.19814/j.jese.2020.04033

He, M. (2007). Distribution and Phytoavailability of Antimony at an Antimony Mining and Smelting Area, Hunan, China. *Environ. Geochem. Health* 29 (3), 209–219. doi:10.1007/s10653-006-9066-9

He, M., and Wan, H. (2004). Distribution, Speciation, Toxicity and Bioavailability of Antimony in the Environment. *Prog. Chem.* 16 (1), 131–135. doi:10.3969/j.issn.1003-5540.2014.03.007

He, M., Wang, N., Long, X., Zhang, C., Ma, C., Zhong, Q., et al. (2019). Antimony Speciation in the Environment: Recent Advances in Understanding the Biogeochemical Processes and Ecological Effects. *J. Environ. Sci.* 75, 14–39. doi:10.1016/j.jes.2018.05.023

He, M., Wang, X., Wu, F., and Fu, Z. (2012). Antimony Pollution in China. *Sci. Total Environ.* 421-422, 41–50. doi:10.1016/j.scitotenv.2011.06.009

Hiller, E., Lalinská, B., Chovan, M., Jurkovič, Ľ., Klimko, T., Jankulár, M., et al. (2012). Arsenic and Antimony Contamination of Waters, Stream Sediments and Soils in the Vicinity of Abandoned Antimony Mines in the Western Carpathians, Slovakia. *Appl. Geochem.* 27 (3), 598–614. doi:10.1016/j.apgeochem.2011.12.005

Jia, H., Qian, H., Zheng, L., Feng, W., Wang, H., and Gao, Y. (2020). Alterations to Groundwater Chemistry Due to Modern Water Transfer for Irrigation over Decades. *Sci. Total Environ.* 717, 137170. doi:10.1016/j.scitotenv.2020.137170

Jiang, N., Li, X., Zhou, A., Huang, Y., and Pan, G. (2020). Effect of pH Value and Fe(Ⅲ) on the Oxidative Dissolution of Stibnite. *Geol. Sci. Technol. Inf.* 39 (4), 76–84. doi:10.19509/j.cnki.dzkq.2020.0410

Leuz, A.-K., Hug, S. J., Wehrli, B., and Johnson, C. A. (2006a). Iron-mediated Oxidation of Antimony(III) by Oxygen and Hydrogen Peroxide Compared to Arsenic(III) Oxidation. *Environ. Sci. Technol.* 40 (8), 2565–2571. doi:10.1021/es052059h

Leuz, A.-K., Mönch, H., and Johnson, C. A. (2006b). Sorption of Sb(III) and Sb(V) to Goethite: Influence on Sb(III) Oxidation and Mobilization. *Environ. Sci. Technol.* 40 (23), 7277–7282. doi:10.1021/es061284b

Liu, J., Jin, D., Wang, T., Gao, M., Yang, J., and Wang, Q. (2019). Hydrogeochemical Processes and Quality Assessment of Shallow Groundwater in Chenqi Coalfield, Inner Mongolia, China. *Environ. Earth Sci.* 78 (12). doi:10.1007/s12665-019-8355-4

Liu, W., Jiang, H., Shi, C., Zhao, T., Liang, C., Hu, J., et al. (2016). Chemical and Strontium Isotopic Characteristics of the Rivers Around the Badain Jaran Desert, Northwest China: Implication of River Solute Origin and Chemical Weathering. *Environ. Earth Sci.* 75 (15), 1119. doi:10.1007/s12665-016-5910-0

Liu, X., Liu, J., Ke, Y., Wang, Q., and Yan, X. (2021). Research Progress on Speciation of Antimony in Natural Water. *Chin. J. Nonferrous Met.* 31 (5), 1330–1346. doi:10.11817/j.ysxb.1004.0609.2021-36569

Long, H., Zheng, Y.-j., Peng, Y.-l., and He, H.-b. (2020). Recovery of Alkali, Selenium and Arsenic from Antimony Smelting Arsenic-Alkali Residue. *J. Clean. Prod.* 251, 119673. doi:10.1016/j.jclepro.2019.119673

Loni, P. C., Wu, M., Wang, W., Wang, H., Ma, L., Liu, C., et al. (2020). Mechanism of Microbial Dissolution and Oxidation of Antimony in Stibnite under Ambient Conditions. *J. Hazard. Mater.* 385, 121561. doi:10.1016/j.jhazmat.2019.121561

McCleskey, R. B., Nordstrom, D. K., and Maest, A. S. (2004). Preservation of Water Samples for arsenic(III/V) Determinations: an Evaluation of the Literature and New Analytical Results. *Appl. Geochem.* 19 (7), 995–1009. doi:10.1016/j.apgeochem.2004.01.003

Multani, R. S., Feldmann, T., and Demopoulos, G. P. (2016). Antimony in the Metallurgical Industry: A Review of its Chemistry and Environmental Stabilization Options. *Hydrometallurgy* 164, 141–153. doi:10.1016/j.hydromet.2016.06.014

Ning, Z., Xiao, T., Yang, F., Jia, Y., Sun, J., and He, L. (2011). Antimony Pollution and Sulfur Isotope Study in the Waters of an Antimony Mine Area. *Bull. Mineral. Pet. Geochem.* 30 (2), 135–141. doi:10.3969/j.issn.1007-2802.2011.02.003

Nyirenda, T. M., Zhou, J., Mapoma, H. W. T., Xie, L., and Li, Y. (2015). Hydrogeochemical Characteristics of Groundwater at the Xikuangshan Antimony Mine in South China. *Mine Water Environ.* 35 (1), 86–93. doi:10.1007/s10230-015-0341-9

Qing, Z. (2012). The Present Situation and Developing Trend of Antimony Industry in China. *Hunan Nonferrous Met.* 28 (2), 71–74. doi:10.3969/j.issn.1003-5540.2012.02.020

Ritchie, V. J., Ilgen, A. G., Mueller, S. H., Trainor, T. P., and Goldfarb, R. J. (2013). Mobility and Chemical Fate of Antimony and Arsenic in Historic Mining Environments of the Kantishna Hills District, Denali National Park and Preserve, Alaska. *Chem. Geol.* 335, 172–188. doi:10.1016/j.chemgeo.2012.10.016

Salam, M. A., and Mohamed, R. M. (2013). Removal of Antimony (III) by Multi-Walled Carbon Nanotubes from Model Solution and Environmental Samples. *Chem. Eng. Res. Des.* 91 (7), 1352–1360. doi:10.1016/j.cherd.2013.02.007

Smichowski, P. (2008). Antimony in the Environment as a Global Pollutant: a Review on Analytical Methodologies for its Determination in Atmospheric Aerosols. *Talanta* 75 (1), 2–14. doi:10.1016/j.talanta.2007.11.005

Thomas, J., Joseph, S., Thrivikramji, K. P., Manjusree, T. M., and Arunkumar, K. S. (2013). Seasonal Variation in Major Ion Chemistry of a Tropical Mountain River, the Southern Western Ghats, Kerala, India. *Environ. Earth Sci.* 71 (5), 2333–2351. doi:10.1007/s12665-013-2634-2

Tong, B., Xu, H., and Liu, Z. (2017). Distribution of Global Antimony Resources and Proposals of Exploration Investment for China. *China Min. Mag.* 26 (S1), 5–10. doi:10.3969/j.issn.1004-4051.2017.z1.003

USGS (2020). *Mineral Commodity Summaries 2020*. New york: U.S. Geological Survey, 22–23. doi:10.3133/70140094

Wang, X., He, M., Lin, C., Gao, Y., and Zheng, L. (2012). Antimony(III) Oxidation and Antimony(V) Adsorption Reactions on Synthetic Manganite. *Geochemistry* 72, 41–47. doi:10.1016/j.chemer.2012.02.002

Wang, X., He, M., Xi, J., and Lu, X. (2011). Antimony Distribution and Mobility in Rivers Around the World's Largest Antimony Mine of Xikuangshan, Hunan Province, China. *Microchem. J.* 97 (1), 4–11. doi:10.1016/j.microc.2010.05.011

Wang, Z., Guo, H., Xiu, W., Wang, J., and Shen, M. (2018). High Arsenic Groundwater in the Guide Basin, Northwestern China: Distribution and Genesis Mechanisms. *Sci. Total Environ.* 640-641, 194–206. doi:10.1016/j.scitotenv.2018.05.255

Wen, B., Zhou, A., Zhou, J., Liu, C., Huang, Y., and Li, L. (2018). Coupled S and Sr Isotope Evidences for Elevated Arsenic Concentrations in Groundwater from the World's Largest Antimony Mine, Central China. *J. Hydrology* 557, 211–221. doi:10.1016/j.jhydrol.2017.12.013

Wen, B., Zhou, J., Zhou, A., Liu, C., and Xie, L. (2016). Sources, Migration and Transformation of Antimony Contamination in the Water Environment of Xikuangshan, China: Evidence from Geochemical and Stable Isotope (S, Sr) Signatures. *Sci. Total Environ.* 569-570, 114–122. doi:10.1016/j.scitotenv.2016.05.124

Wilson, S. C., Lockwood, P. V., Ashley, P. M., and Tighe, M. (2010). The Chemistry and Behaviour of Antimony in the Soil Environment with Comparisons to Arsenic: a Critical Review. *Environ. Pollut.* 158 (5), 1169–1181. doi:10.1016/j.envpol.2009.10.045

Xiao, J., Jin, Z. D., Wang, J., and Zhang, F. (2015). Hydrochemical Characteristics, Controlling Factors and Solute Sources of Groundwater within the Tarim River Basin in the Extreme Arid Region, NW Tibetan Plateau. *Quat. Int.* 380-381, 237–246. doi:10.1016/j.quaint.2015.01.021

Xie, L., Zhou, J., Hao, C., Liu, H., Nyirenda, M. T., Lu, J., et al. (2016). Hydrochemical Characteristics and Contaminative Causes of Groundwater in the North Area of Xikuangshan Antimony mine,Hunan Province. *Dizhi Keji Qingbao* 35 (2), 197–202.

Xing, L., Guo, H., and Zhan, Y. (2013). Groundwater Hydrochemical Characteristics and Processes along Flow Paths in the North China Plain. *J. Asian Earth Sci.* 70-71, 250–264. doi:10.1016/j.jseaes.2013.03.017

Zhang, L., Song, B., Huang, F., Xiao, N., and Dun, M. (2022). Characteristics of Antimony Migration and Transformation and Pollution Evaluation in a Soil-Crop System Around a Tin Mine in Hunan Province. *Environ. Sci.* 43 (3), 1558–1566. doi:10.13227/j.hjkx.202105162

Zhou, J., Nyirenda, M. T., Xie, L., Li, Y., Zhou, B., Zhu, Y., et al. (2017). Mine Waste Acidic Potential and Distribution of Antimony and Arsenic in Waters of the Xikuangshan Mine, China. *Appl. Geochem.* 77, 52–61. doi:10.1016/j.apgeochem.2016.04.010

Zhu, B., Yang, X., Rioual, P., Qin, X., Liu, Z., Xiong, H., et al. (2011). Hydrogeochemistry of Three Watersheds (The Erlqis, Zhungarer and Yili) in Northern Xinjiang, NW China. *Appl. Geochem.* 26 (8), 1535–1548. doi:10.1016/j.apgeochem.2011.06.018

Zhu, J., Wu, F., Deng, Q., Shao, S., Mo, C., Pan, X., et al. (2009). Environmental Characteristics of Water Near the Xikuangshan Antimon Mine, Hunan Province. *Acta Sci. Circumstantiae* 29 (3), 655–661. doi:10.13671/j.hjkxxb.2009.03.002

Conflict of Interest: Authors XS and CH are employed by North China Institute of Science and Technology. Authors YL, LZ, and ZL are employed by Hebei Geo-Environment Monitoring. Author CL is employed by Liaoning Metallurgical Geological Exploration Research Institute Co. Ltd.